Crustal and Upper Mantle Velocity Model along the DOBRE-4 Profile from North Dobruja to the Central Region of the Ukrainian Shield : 1. Seismic Data

Starostenko, V. I.

2017-03

Starostenko , V I , Janik , T , Gintov , O B , Lysynchuk , D V , Sroda , P , Czuba , W , Kolomiyets , E V , Aleksandrowski , P , Omelchenko , V D , Komminaho , K , Guterch , A , Tiira , T , Gryn , D N , Legostaeva , O V , Thybo , G & Tolkunov , A V 2017 , ' Crustal and Upper Mantle Velocity Model along the DOBRE-4 Profile from North Dobruja to the Central Region of the Ukrainian Shield : 1. Seismic Data ' , Izvestiya, Russian Academy of Sciences. Physics of the Solid Earth , vol. 53 , no. 2 , pp. 193-204 . https://doi.org/10.1134/S1069351317020124

http://hdl.handle.net/10138/312484
https://doi.org/10.1134/S1069351317020124

publishedVersion

ISSN 1069-3513, Izvestiya, Physics of the Solid Earth, 2017, Vol. 53, No. 2, pp. 193–204. © Pleiades Publishing, Ltd., 2017.
Original Russian Text © V.I. Starostenko, T. Janik, O.B. Gintov, D.V. Lysynchuk, P. Środa, W. Czuba, E.V. Kolomiyets, P. Aleksandrowski, V.D. Omelchenko, K. Komminaho, A. Guterch, T. Tiira, D.N. Gryn, O.V. Legostaeva, G. Thybo, A.V. Tolkunov, 2017, published in Fizika Zemli, 2017, No. 2, pp. 24–35.

Crustal and Upper Mantle Velocity Model along the DOBRE-4 Profile from North Dobruja to the Central Region of the Ukrainian Shield: 1. Seismic Data

V. I. Starostenko[a, *], T. Janik[b, **], O. B. Gintov[a], D. V. Lysynchuk[a], P. Środa[b], W. Czuba[b], E. V. Kolomiyets[a], P. Aleksandrowski[c, *], V. D. Omelchenko[a], K. Komminaho[d], A. Guterch[b], T. Tiira[d, ****], D. N. Gryn[a], O. V. Legostaeva[a], G. Thybo[e, *****], and A. V. Tolkunov[f, ******]**

[a] *Institute of Geophysics, National Academy of Sciences of Ukraine, Kiev, Ukraine*
[b] *Institute of Geophysics, Polish Academy of Sciences, Warsaw, Poland*
[c] *Polish Geological Institute—National Research Institute, Wroclaw, Poland*
[d] *Institute of Seismology, University of Helsinki, Helsinki, Finland*
[e] *Department of Geography and Geology, University of Copenhagen, Copenhagen, Denmark*
[f] *State Geophysical Enterprise Ukrgeofizika, Kiev, Ukraine*
** e-mail: vstar@igph.kiev.ua*
***e-mail: janik@igf.edu.pl*
****e-mail: pale@pgi.gov.pl*
*****e-mail: Timo.Tiira@helsinki.fi*
******e-mail: THYBO@geol.ku.dk*
*******e-mail: geolog@ukrgeofizika.kiev.ua*

Received February 21, 2016

Abstract—For studying the structure of the lithosphere in southern Ukraine, wide-angle seismic studies that recorded the reflected and refracted waves were carried out under the DOBRE-4 project. The field works were conducted in October 2009. Thirteen chemical shot points spaced 35–50 km apart from each other were implemented with a charge weight varying from 600 to 1000 kg. Overall 230 recording stations with an interval of 2.5 km between them were used. The high quality of the obtained data allowed us to model the velocity section along the profile for *P*- and *S*-waves. Seismic modeling was carried out by two methods. Initially, trial-and-error ray tracing using the arrival times of the main reflected and refracted *P*- and *S*-phases was conducted. Next, the amplitudes of the recorded phases were analyzed by the finite-difference full waveform method. The resulting velocity model demonstrates a fairly homogeneous structure from the middle to lower crust both in the vertical and horizontal directions. A drastically different situation is observed in the upper crust, where the *V*p velocities decrease upwards along the section from 6.35 km/s at a depth of 15–20 km to 5.9–5.8 km/s on the surface of the crystalline basement; in the Neoproterozoic and Paleozoic deposits, it diminishes from 5.15 to 3.80 km/s, and in the Mesozoic layers, it decreases from 2.70 to 2.30 km/s. The subcrustal *V*p gradually increases downwards from 6.50 to 6.7–6.8 km/s at the crustal base, which complicates the problem of separating the middle and lower crust. The *V*p velocities above 6.80 km/s have not been revealed even in the lowermost part of the crust, in contrast to the similar profiles in the East European Platform. The Moho is clearly delineated by the velocity contrast of 1.3–1.7 km/s. The alternating pattern of the changes in the Moho depths corresponding to Moho undulations with a wavelength of about 150 km and the amplitude reaching 8 to 17 km is a peculiarity of the velocity model.

DOI: 10.1134/S1069351317020124

1. INTRODUCTION

This paper addresses the results of the deep seismic sounding (DSS) experiment DOBRE-4 (Starostenko et al., 2013) conducted in Ukraine in 2009, which was aimed at studying the overall structure of the Earth's crust and upper mantle within the southeastern part of the East European platform (EEP), including its transition to the Trans-European suture zone. The wide-angle seismic reflection and refraction (WARR) method is a reliable and sufficiently accurate instrument for achieving this objective. This method yields the distributions of the seismic velocities, reveals variations in the thickness and the fault-block structure of the crust, identifies the waveguides and core-to-mantle transition zones; i.e., it reconstructs the structure

of the deep tectonic zones in the upper part of the lithosphere.

At the first stage of the interpretation of the DOBRE-4 seismic data (Starostenko et al., 2013), he Moho topography was accounted for by the hypothetical crumpling of the cold lithosphere with the relatively strong mantle based on the hypothesis of biharmonic uncoupled folding (Cloetingh et al., 1999). In the present work, the analysis of the geological nature of the velocity section on the DOBRE-4 profile is based on the plate tectonic model of the evolution of the lithosphere.

The position of the profile along which the seismic DOBRE-4 experiment was carried out is shown in Fig. 1. The profile with a length of ~500 km starts from the Ukrainian–Romanian boundary near the town of Reni on the River Danube, then runs northeastwards along the Black Sea coastal plain, where it passes about 30 km northwest of Odessa and ends north of Krivoi Rog. In the southwest, the profile starts within the Lower Prut Horst of Northern Dobruja (LPHND) (shot point SP 15100), and intersects the Pre-Dobruja Depression (PDD) (shot points (SP) SP 15101–SP 15103), South Ukrainian Monocline (SUM) (shot points SP 15103–SP 15108, previously referred to as the Cis-Black-Sea Depression), and the southern slope of the Ukrainian Shield (USh) covered by the sediments in the interval of shot points SP 15108–SP 15109 and exposed in the interval of SP 15110–SP 15112. The profile ends within the Krivoi Rog–Kremenchug fault zone. DOBRE-4 is the fourth profile in the series of international DSS profiles which have been acquired in Ukraine since 1999 for studying the deep structure of the Earth crust and upper mantle in the southern part of the EEP.

The region of the work has been previously extensively surveyed by the geophysical methods, including several DSS profiles. The Geotraverse VII (Sollogub et al., 1988) which is subparallel to and located near the DOBRE-4 profile was studied in the 1970s. It was acquired by the DSS and common depth point (CDP) methods. Geotraverses IV and VI (Fig. 1) illuminate the part of the USh which has subsequently become the object of study of the DOBRE-4 experiment. Several seismic DSS profiles were acquired in the region of Krivoi Rog for exploring the Moho and constructing the 3D crustal model in the region of the Krivoi Rog superdeep borehole (*Glubinnoe ...*, 2004; Starostenko et al., 2007). The deep structure of the folded belt of Northern Dobruja was studied under the VRASNCEA-2001 project (Hauser et al., 2007).

All the previous studies were mainly based on the records of the reflected seismic phases, which unfortunately provide little information about the velocity distribution in the lithosphere. The modern seismic stations used in the DOBRE experiments provided the traveltime curves for both reflections and refractions at the significantly larger offsets, which enabled the geophysicists to reconstruct more elaborate models of the velocity and crustal structure. At the same time, the previous seismic studies were conducted with sufficiently greater detail; for example, the receiver spacing was from 100 m, which made it possible to recognize the relatively short individual reflectors and to identify, against their background, the steep and gently dipping faults. Therefore, the joint analysis of the DOBRE-4 data and the results of the previous works can promote a geological interpretation of the seismic experiment. In the case of the DOBRE-4 profile, such a possibility exists due to the previous DSS studies on geotraverse VIII in this region (Sollogub, 1986).

The field acquisition in DOBRE-4 experiment was conducted at the beginning of October, 2009 and included 13 shot points (SP) with a distance of 30–50 km between them, as well as the 230 seismic recording stations which were installed every 2.5 km. One-hundred-and-seventy-four wells were used for placing a total of 8700 km of chemical explosives (TNT).

The DOBRE-4 project is the result of combined international efforts contributed by Ukraine (Institute of Geophysics of the National Academy of Sciences of Ukraine and State Geophysical Enterprise Ukrgeofizika, Kiev), Denmark (Geological Institute at the University of Copenhagen), Finland (Institute of Seismology at the University of Helsinki), and Poland (Institute of Geophysics of the Polish Academy of Sciences).

2. SEISMIC DATA

Several phases of compressional *P*- and shear *S*-waves were identified in the seismic records. These phases were subsequently used in modeling. The seismic records reflect the complicated structure of the wave field, particularly the Moho reflections testifying to changes in the Moho structure along the profile. The seismic sections are shown in Figs. 2a, 2b, and 3c.

2.1. P-Waves. Refractions

The first arrivals of the *P*-waves are the refractions from the upper layers of the sediments (*P*sed), upper/middle crystalline crust (*P*g), and upper mantle refractions (*P*n). For most shot points, the first arrivals can be correlated on the offsets up to 200–210 km (*P*g) and about 400 km (refracted mantle phases).

The *P*sed phases—refractions in the upper crustal sedimentary layers—are observed in the southern part of the profile (SP 15000–15004) at the offsets of 0–10 km with apparent velocities within 2.3–3 km/s.

At the long offsets (10 to 200 km), phases *P*g are observed with the apparent velocity of 5.5–6.2 km/s, which indicates their origin from the refraction at the consolidated (crystalline?) basement. The *P*g phases in the southern part of the profile (SP 15100–15104) have the apparent velocity of 5.5–5.7 km/s (up to the offsets of 50 km) and 6.3–6.4 km/s (at the offsets of

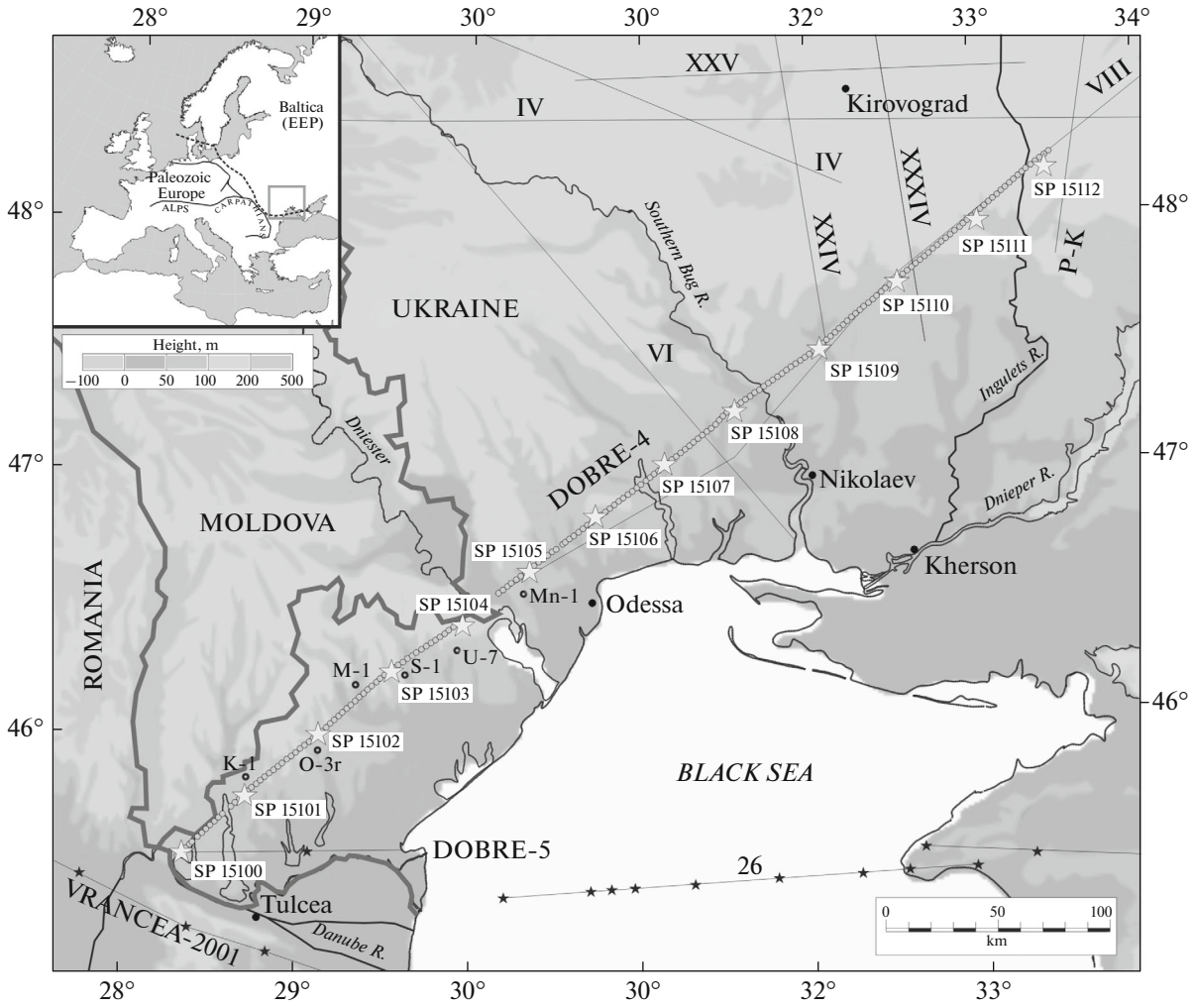

Fig. 1. The position of the DOBRE-4 profile and previous seismic experiments on the physical map. The large asterisks denote the shot points; the gray circles denote the recording stations; the small asterisks denote the shot points of VRANCEA-2001, DOBRE-5, and the recording stations of profile 26 (marine part of DOBRE-5); the black lines with roman numerals denote the old DSS geotraverses; and the gray lines delineate the state boundaries. Boreholes: K-1, Krasnoarmeiskaya-1 (5.4 km NW of the profile); O-3P, the Orekhovskaya-3P (5.6 km SW); M-1, Mirnopolskaya-1 (4.2 km NW); S-1, Saratskaya-1 (5 km SE); U-7, Uspenskaya-7; Mn-1, Mirnenskaya-1. The position of the study region is shown in the inset. The Teisseyre-Tornquist zone is shown by the dashed line.

50–100 km). In the north (SP 15105–15111) at the offsets of 50–100 km, the *P*g phases have apparent velocities of 5.8–6.1 km/s which increase up to 6.2–6.3 km/s in the interval of the offsets from 50–150 to 100–200 km.

The crustal refractions which are traced in the subsequent arrivals (*P*ov) at the offsets of 200–300 km have the apparent velocity of 6.4–6.5 km/s.

The mantle phases (P_{mantle}) are observed at several SPs at the offsets of 200–400 km, in some cases with very high amplitudes (e.g., SP 15104). Their apparent velocity varies within 8–8.3 km/s. These phases represent the Moho refractions (*P*n), reflections for the mantle heterogeneities (P_1P, P_2P), and probably separate diffracted phases. Since phase identification was not possible until the modeling stage, the phases are discussed in Section 5.

2.2. Reflections

The reflecting properties of the crust differ along the profile. In the southern part at a distance 0–265 km the *P*g arrivals and reflected phases are characterized by strong incoherent codas with a duration of a few seconds, which testifies to the fairly low reflecting properties of the crust (SP 15101). In the northern part, the *P*g arrivals are sharp and short series of waves followed by weak codas, sometimes with the amplitudes only slightly above the background noise (SP 15109, SP 15111). This means that the crust is almost transparent for the seismic waves except for several phases

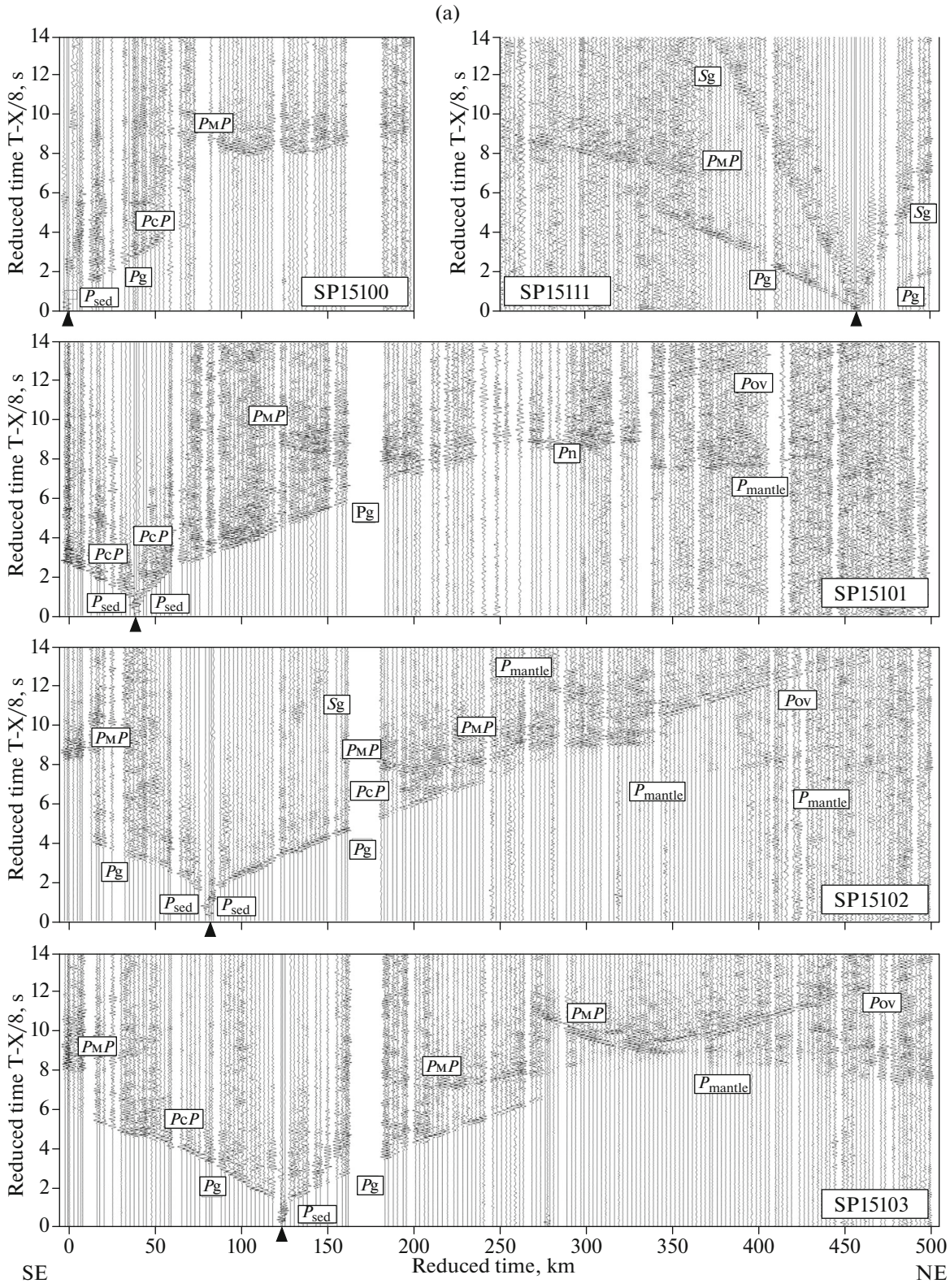

Fig. 2. The normalized seismic records of the vertical *P*-wave component (SP 15100–SP 15103, SP 15111) filtered in the frequency band 2–12 Hz. *P*g is the refractions in the upper and middle crust; *P*ov are the overcritical crustal phases; *PcP* are the reflected phases in the middle crust; P_MP are the Moho reflections; *P*n are the upper mantle refractions; and $P_{mantle}P$ are the upper mantle *P*-wave phases. The reduced velocity is 8.0 km/s. Figures 2b and 2c are a continuation of Fig. 2.

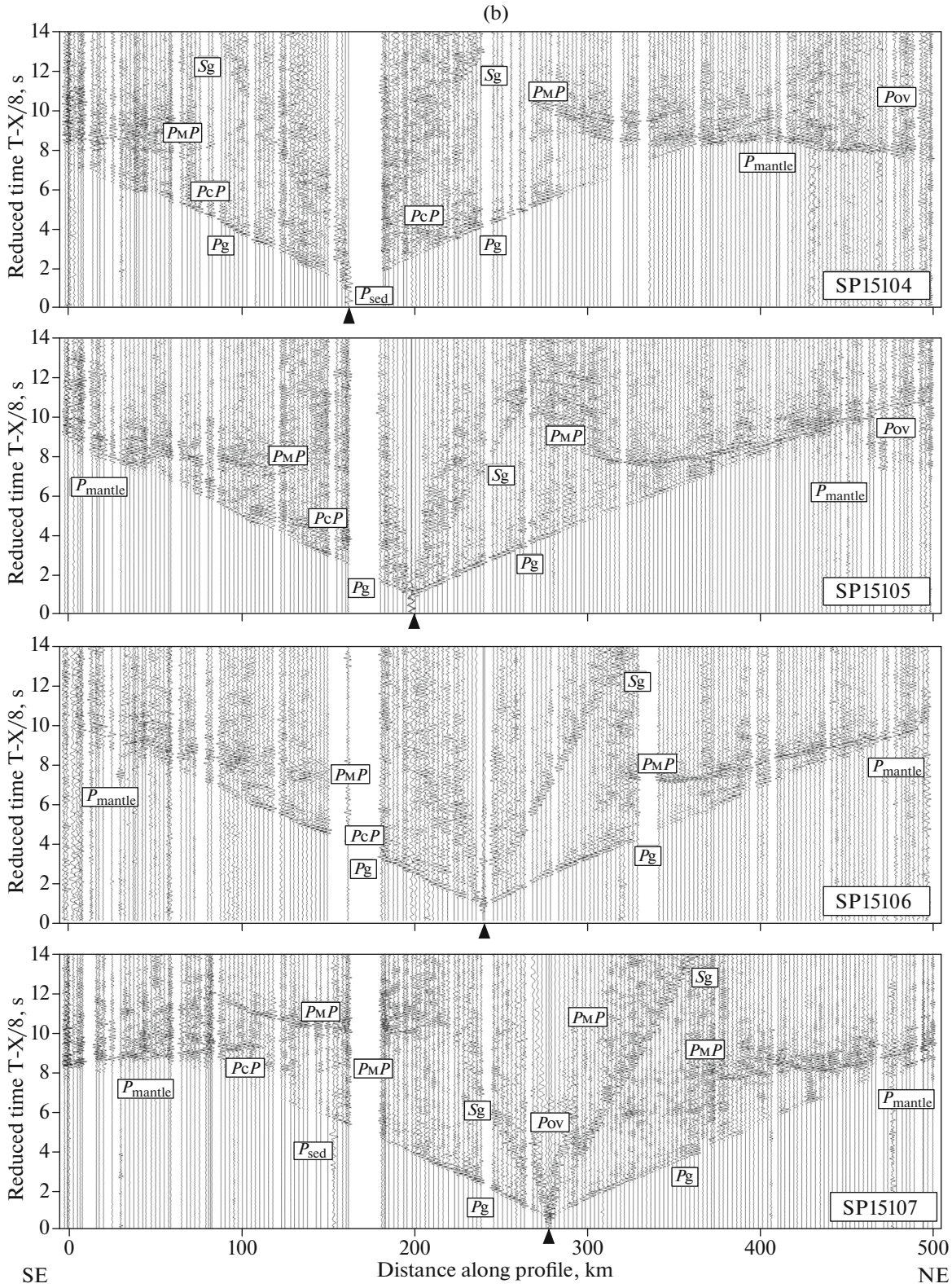
(b)
Reduced time T-X/8, s
Sg
PMP
PcP
Pg
Psed
Pov
Pmantle
SP15104
SP15105
SP15106
SP15107
0
100
200
300
400
500
SE
NE
Distance along profile, km

Fig. 2. (Contd.).

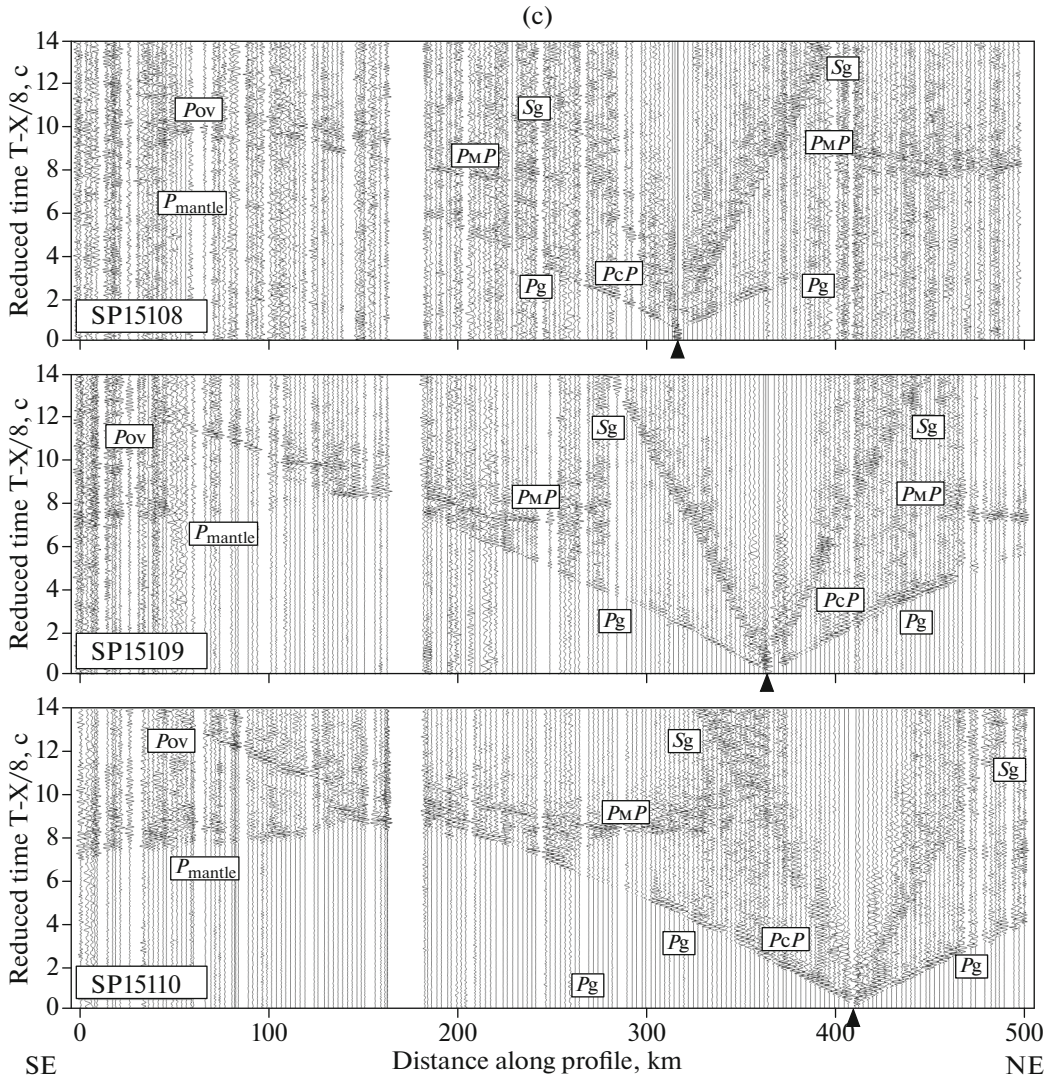

Fig. 2. (Contd.).

received from the fragments of the larger-scale velocity discontinuities. The contrast in the pattern of the waves is most clearly pronounced in the SP 15105 section, where phases *P*g and P_MP have different characteristics south and north of the shot point. This can be associated with the complicated structure of the sedimentary cover whose thickness increases southwards or with the more intense crustal deformations in the southern part.

Coherent reflections from velocity discontinuities in the upper/middle crust are rare. The deep reflections are interpreted as produced on the top of the lower crust and are correlated on the short (~20 km) offsets for a few SPs only (SPs 15101, 15106, and 15110).

The highly coherent reflections with extremely high amplitudes observed at 7–9 s (reduced time) at the offsets of 100–250 km are the most striking feature. In the seismograms, on both ends of the profile, these reflections appear as the typical single P_MP phases (reflections from the Moho discontinuity). In the other seismograms, we frequently observe two separate phases with lower and higher apparent velocities, which intersect each other (e.g., SP 15103) or arrive at a different reduced time (e.g., SP 1507), with one reflection from the Moho at a reduced time of ~8 s and the other deep reflection at a reduced time of ~10 s.

The direct seismic modeling has shown that these double phases are reflections from a strongly undulating Moho discontinuity. The fragments of the traveltime curves with high apparent velocity were formed on the Moho segments which rise with increasing offsets, whereas the phases with lower velocity arrive from the Moho segments whose depth grows with increasing offset. They all form the characteristic tripling of the traveltime curve (e.g., SP 15101, SP 15103, and SP 15105 in Figs. 2a and 2b). As a rule, these phases

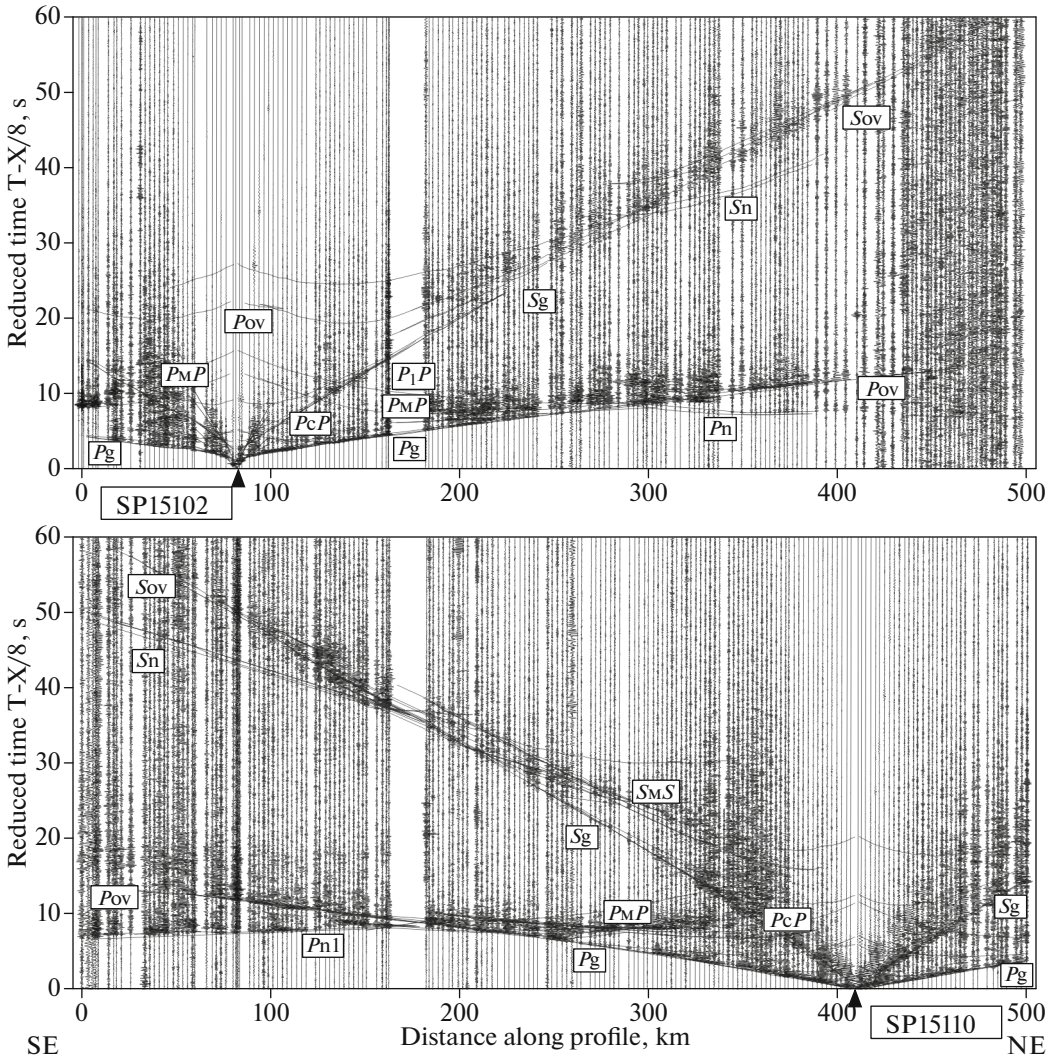

Fig. 3. The normalized seismic traces of the common shot point with the records of the vertical components of the *P*- and *S*-waves for SP 151002 and SP 151010. 1–8 Hz bandpass filtering and reduced velocity of 8.0 km/s are used.

have a very high quality; therefore, despite their untypical character, they can be identified highly reliably.

2.3. S-Waves

The *S*-wave arrivals have a lower quality than the *P*-phases. Generally, they have a higher amplitude in the northern part of the profile, probably due to the thinning sedimentary cover. The *S*-phase arrivals are more fragmented than the *P*-phases. They are overlapped by the *P*-codas and are not constantly traced. For SPs 15100 and 15101 in the south, the *S*g phase is not seen at all; however, the S_MS arrivals can be correlated. For the other SPs, the *S*g phase has a different quality, whereas S_MS typically has a higher amplitude. In some seismograms (e.g., SP 15103), a certain increase in the amplitude at offsets of more than 200 km indicates weak upper-mantle refraction (*S*n phase). The most clearly pronounced *S*-waves traced at SP 15102 and SP 15110 are shown in Fig. 3.

3. SEISMIC MODELING METHODS

The seismic data were used for the modeling by two methods. Initially, ray tracing by the successive approximation technique was conducted. Next, the amplitudes and phases were analyzed by the finite-difference full waveform calculations.

The ray-tracing calculations were conducted with the use of the SEIS3 program package (Červený and Pšenčík, 1984), together with the MODEL (Komminaho, 1998) and ZPLOT (Zelt, 1994) graphical applications. The algorithm implementing this technique includes the calculation of ray paths, traveltimes, and synthetic seismograms in a high-frequency approxi-

mation. The model consists of layers with gradually varying velocities, which are separated by velocity discontinuities (Fig. 4). In each layer, the *P*-wave velocity is parameterized on an irregular rectangular grid and interpolated by bicubic splines. Velocity discontinuities are allowed within the layers. In the preparation of the initial input model, the velocity distribution in the upper crust was constrained based on the geological and geophysical data obtained in the boreholes and in the seismic studies in the neighboring regions. The search for the solution was conducted interactively: the traveltime curve calculated for the current *P*-wave model was compared to the observed traveltime curve to minimize the misfit. Modeling also included the calculation of synthetic seismograms and comparison of the amplitudes of the synthetic and observed data. This provided additional constraints for the gradients and velocity contrasts at the discontinuities.

As a rule, the ray-tracing algorithm calculates the traveltime curves and yields the velocity model. For the DOBRE-4 this approach proved to be highly efficient for the crustal velocity model; however, the Moho topography (e.g., the depth difference by ~13 km over a horizontal distance ~50 km) precluded us from calculating the theoretical traveltime curves of the refracted waves in the mantle (the steep descent of the boundaries and deep troughs produce shadow zones in the ray-tracing approximation of the wave paths). Hence, the velocity distribution in the upper mantle was modeled in parallel by two methods.

The first method only used the algorithm of ray theory. Velocity discontinuities were specified in such a way that the rays of the reflected waves were as close as possible to the rays of the refracted waves in the shadow zones and, hence, emulated the *P*n-phases.

The second method used the full waveform modeling in order to overcome the limitations of the ray-tracing technique. Routine computations of the runtime model versions used the MPM program (Hansen and Jacobsen, 2002), whereas the final versions of the synthetic velocity sections were calculated by the Tesseral 2–D package (Kostyukevich et al., 2000). The synthetic seismograms calculated in this way made it possible to obtain the traveltimes of the mantle phases even in the previously shaded zones, which were subsequently compared to the empirical data. As a result, the mantle structure without the boundary shown by the dashed line in Fig. 4 was obtained, whereas at the stage of phase correlating the full waveform modeling significantly promoted the correct identification of the observed mantle phases in the intervals with a complicated MOHO topography.

4. VELOCITY MODEL FROM *P*- AND *S*-WAVES

The direct wave field modeling for 13 SPs from the *P*- and *S*-waves yielded the velocity model for the *P*-waves and the V_p/V_s velocity ratio distribution along the 505-km DOBRE-4 profile. In the southwestern part, the starting model is based on the well logging data from six boreholes with depths ranging from 1.5 to 3.5 km, located at a distance of 5.6 km from the profile. The model is shown in Fig. 4.

4.1. Earth's Crust

In the sedimentary cover with a thickness of 0.5–4.2 km, the velocities mainly fluctuate between 2.3 and 5.45 km/s. Sedimentary layers with V_p velocities of 2.3–4.75 km/s and thickness of ~1 km are stretched by ~360 km northeast. These sediments are underlain by a layer with a thickness of 1–2 km, *P*-velocities of 5.1–5.15 km/s, and velocity ratio $V_p/V_s = 1.52–1.55$. Farther northeast, within USh, this layer with slightly higher velocities of 5.45 km/s and $V_p/V_s = 1.71$ becomes shallower, almost reaching the surface. Its thickness varies from 0–1.3 km beneath the Ingul megablock to 0.25 km beneath the Ingulets-Krivoi Rog suture zone and the central area of the Middle-Cis-Dnieper megablock.

An important structural element in the sedimentary cover is the deep (with an amplitude of at least 3 km) depression with a width of 40 km, *P*-wave velocities 2.3, 2.7, 3.75, and 4.75 km/s, and $V_p/V_s = 1.55$ observed within the PDD.

The crystalline rocks are composed of four layers. The *P*-wave velocities in the three upper layers are 5.8–6.0, 6.1–6.2, and 6.3–6.35 km/s, and the velocity ratio V_p/V_s is 1.66–1.71, 1.68–1.71, and 1.71, respectively.

4.2. The Moho and Upper Mantle

The direct ray tracing has shown that some parts of the mantle phases are refractions on the Moho heterogeneities (*P*n phases). At the same time, the other waves in the mantle (e.g., SP 15101 in the interval 320–490 km) appear to have been formed in a different way. The refracted waves are observed at distances where the ray optic predicts the existence of shadow zones due to the significant contrasts in the Moho depths. Therefore, modeling these phases by the ray method alone is barely practicable because this method implies the comparison of the calculated and observed traveltime curves. In order to overcome this limitation of the ray-tracing modeling, we used the full waveform modeling the mantle phases.

The model demonstrates significant contrasts in the Moho depths. Within the Trans-European Suture Zone (TESZ) (up to 80 km from the beginning of the profile), the Moho is virtually flat at a depth of 39 km. In the next part of the profile, at a distance of ~360 km, mainly beneath the SUM and partly beneath the USh, the Moho has two large inhomogeneities. The most intense change in the Moho depth is observed in the interval from a depth of 32 km at the distance of 165 km from the beginning of the profile to a depth of 48 km

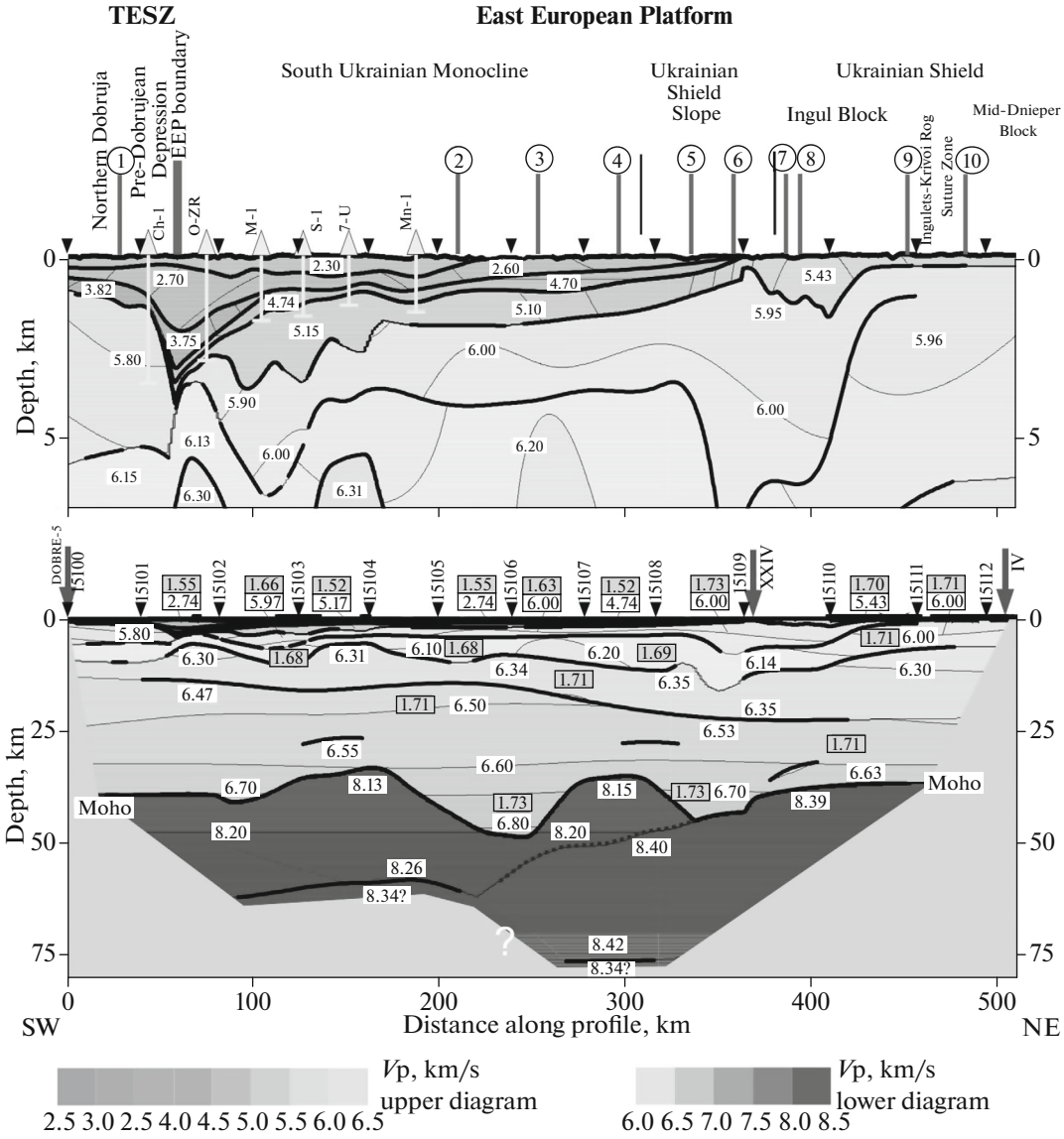

Fig. 4. 2D velocity model along the DOBRE-4 profile. The upper diagram shows the sedimentary cover on an enlarged vertical scale. The lower panel presents the model obtained based on the modeling results using the SEIS83 program (Červený and Pšenčík, 1984). The boundary shown by the dashed line in the upper mantle is obtained by the full waveform modeling program MPM (Hansen and Jacobsen, 2002). The ray tracing and full waveform modeling are conducted with the same structural model of the section. TESZ stands for the Trans European Suture Zone. The thick black lines show the main velocity boundaries. The thin black lines show the contours of equal velocities; the corresponding velocity values (in km/s) are indicated in the white boxes. The names of the large tectonic blocks are indicated above the model. The black triangles show the locations of the shots; the gray arrows show the intersections with the other profiles. The vertical axis is enlarged by a factor of 6.7 for the sedimentary cover and by a factor of 2.4 for the full model. The data for the V_p/V_s ratio are shown in the gray boxes.

at a distance of 250 km. At a distance of 300 km, the Moho again rises up to 35 km. Further northeast there is a small depression in the Moho (the depth is 44 km) beneath the southern margin of the USh. Further on, beneath the shield closer to the end of the profile, the Moho becomes slightly shallower up to a depth of 36 km (at a distance of 450 km).

The sub-Moho velocities are ~8.15 km/s in the southwestern and central parts of the profile. Beneath the USh, starting from a distance of 330 km, they are higher (8.3 km/s). The upper mantle model obtained by the ray-tracing technique has an important feature: the mantle boundaries in the central part of the profile subside from a depth of 50 km at a distance of 340 km to a depth of 60 km at a distance of 240 km. This feature separates the regions with relatively low (8.15–8.25 km/s) and high (8.3–8.4 km/s) velocities. An alternative solution is obtained for the model where the dashed boundary (Fig. 4) is replaced by a zone with gradually varying velocity. This version was

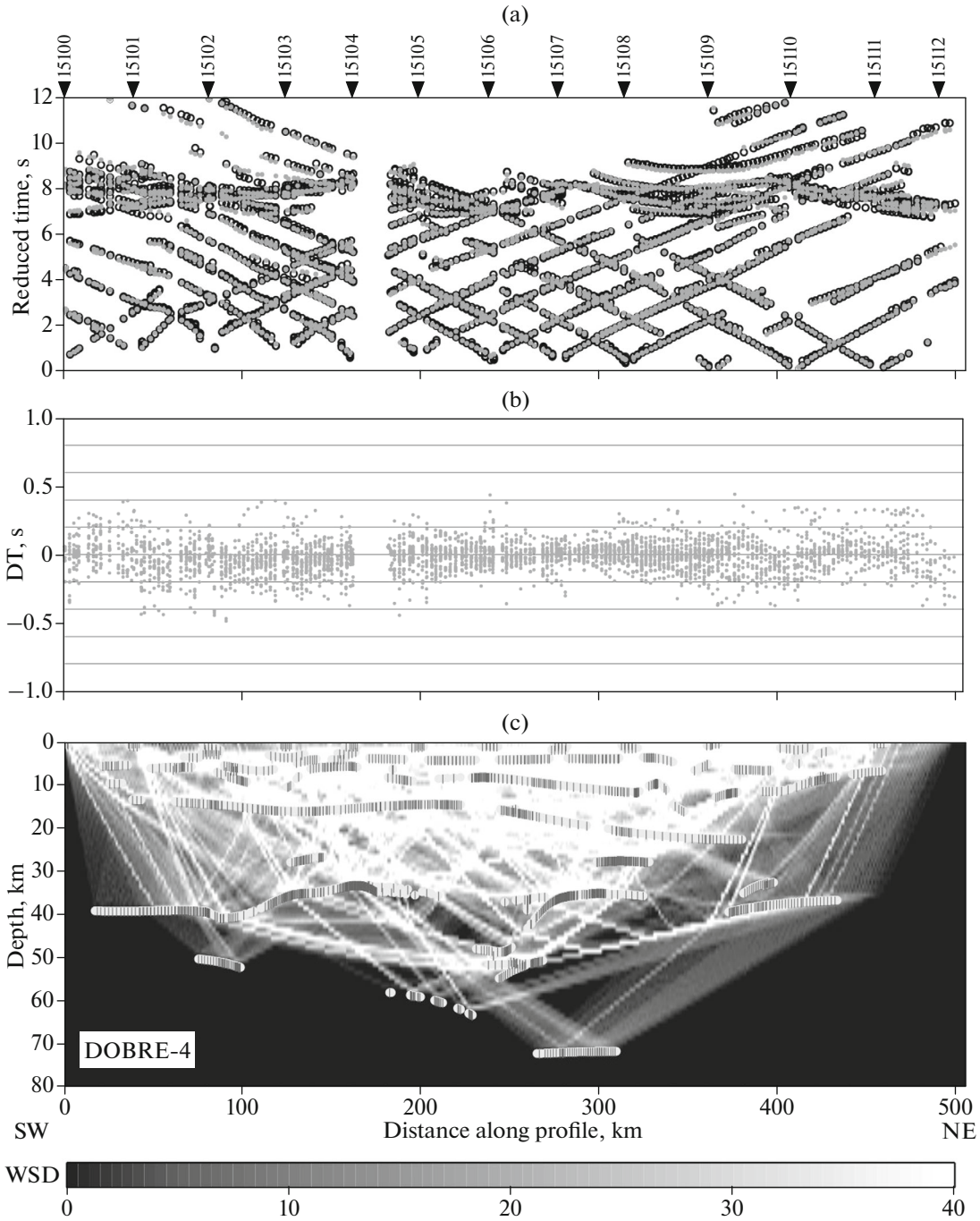

Fig. 5. (a) The diagrams showing the theoretical and observed traveltime curves; (b), the time differences between them; (c) the ray coverage for the direct ray-tracing modeling on the DOBRE-4 profile. The gray dots in the upper diagram show the observed arrivals; the black dots show the calculated arrivals at the same distances. The gray lines with vertical strokes in the lower diagram depict the fragments of velocity boundaries obtained from reflected waves. The strokes along the boundaries indicate the presence of the detected reflected phases in the section (every third point shown); the density of the strokes is the measure of positioning accuracy of the reflectors. WSD is the weighted summation derivative characterizing the density of ray coverage.

yielded by the full waveform modeling technique. The highest velocity (8.4 km/s) in the upper mantle is observed at a distance of 260–315 km up to a depth of 70 km. Besides, several reflectors are also observed in the upper mantle beneath the EEP approximately 20–30 km below the Moho at the depths of ~60 and 75 km.

5. THE ANALYSIS OF THE ACCURACY FOR THE MODEL OBTAINED BY THE RAY METHOD

Timing and positioning the SPs and seismic stations was carried based on GPS technologies with an accuracy of 1 ms and dozens of meters, respectively.

These errors are negligible compared to the characteristic scales of the experiment on the study of the Earth's crust. The uncertainty in the velocities and depths in the model obtained by the ray method primarily originates from the errors of the subjective detection of the peak phases in the time section. These errors are within 0.1 s. However, the uncertainty decreases with the improvement of the quality and with the growth of the amount of data (the number of explosions and receivers, the efficiency of the shot sources, the signal-to-noise ratio, the possibility of checking the time at the reciprocity points of the branches of the traveltime curves, and coverage of the model by the rays of the detected waves).

The high data quality and thorough interpretation enabled us to construct the model yielding the theoretical traveltime curves that highly accurately coincide with the observed curves for both the reflected and refracted waves. Several tests were conducted for estimating the ambiguity in the model parameters. These tests were carried out, e.g., in (Janik et al., 2002; 2009; Środa et al., 2006). The diagrams showing the calculated and observed traveltime curves with ray coverage, as well as the residuals between the calculated and observed traveltimes, are presented in Fig. 5. The root mean square (RMS) deviations are acceptable and are 0.36 for sediments, 0.21 for the crust, 0.17 for the Moho reflections (P_MP), 0.31 for the refracted phases Pn, and 0.74 for all the reflections in the upper mantle. The RMS value for the crustal refracted phases is 0.11, whereas in the case of the reflected phases, it is 0.30. The overall RMS value for 3880 traveltime peaks is 0.37. This means that the calculated traveltime curves for the refracted phases in the Earth's crust coincide closer with the empirical data than the reflected ones. The traveltime curves for the Moho were modeled better than for the intracrustal reflections.

6. CONCLUSIONS

A large-scale wide-angle seismic experiment was carried out in the southeastern part of Ukraine. The aim of the experiment was to study the deep structure of the Earth's crust and upper mantle. The high quality of seismic data allowed us to document the structures of the LPHND, PDD, SUM, the southern slope, and the outcropped part of USh.

The velocity model on the DOBRE-4 profile includes the sedimentary layers with Vp ≈ 2.6–4.7 km/s represented by the Ordovician–Jurassic terrigenous-clayey and lime formations. They are present all over the LPHND, PDD, and SUM.

The basement beneath the LPHND consists of a single layer with Vp ≈ 5.8 km/s, which differs from the PDD where there are two layers with Vp = 5.10–5.15 and Vp ≤ 6.0 km/s, respectively.

Based on the seismic data, two Moho depressions on the lithospheric scale were revealed. The first depression is located between SP 5108 and SP 15109. Here the crustal thickness reaches 45 km. The crustal Vp ≈ 6.7 km/s sharply changes in the Moho to Vp ≈ 8.4 km/s in the mantle. The depression is different from the one presented on Geotraverse VIII and in the DOBRE-4 profile between SP 15105 and SP 15106, where the crustal thickness is 57 km and the mantle velocities are 8.2 km/s.

The mantle depression between SP 15105 and SP 15106 corresponds to GSZ. A similar depression is also established on geotraverses IV and VIII beneath IKRSZ. The DOBRE-4 velocity section of the mantle and neighboring mantle allows us to gain a more detailed idea concerning the geodynamical model of the formation of the southwestern EEP part in the early Precambrian from the plate tectonic standpoint. This issue will be discussed in detail in the second part of the paper.

REFERENCES

Červený, V. and Pšenčík, I., SEIS83—Numerical modelling of seismic wave fields in 2-D laterally varying layered structures by the ray method, in *Documentation of Earthquake Algorithms. Rep. SE-35*, Engdal, E.R., Ed., Boulder: World Data Center A for Solid Earth Geophysics, 1984, pp. 36–40.

Cloetingh, S., Burov, E., and Poliakov, A., Lithosphere folding: primary response to compression? (from Central Asia to Paris Basin), *Tectonics*, 1999, vol. 18, pp. 1064–1083.

Glubinnoe stroenie i seismichnost' Karel'skogo regiona i ego obramleniya (Deep Structure and Seismicity of the Karelian Region and Its Framing), Sharov, N.V, Ed., Petrozavodsk: Inst. Geol. Karel. NTs, RAN, Min. prirod. resursov, FGU GNPP Spetsgeofizika, 2004.

Hansen, T.M. and Jacobsen, B.H., Efficient finite difference waveform modeling of selected phases using a moving zone, *Comput. Geosci.*, 2002, vol. 28, no. 7, pp. 819–826.

Hauser, F., Railean, V., Fielitz, W., et al., Seismic crustal structure between the Transylvanian Basin and the Black Sea, Romania, *Tectonophysics*, 2007, vol. 430, pp. 1–25.

Janik, T., Yliniemi, J., Grad, M., Thybo, H., Tiira, T., and POLONAISE P2 Collab., Crustal structure across the TESZ along POLONAISE'97 seismic profile P2 in NW Poland, *Tectonophysics*, 2002, vol. 360, pp. 129–152.

Janik T., Grad M., Guterch, A., and CELEBRATION 2000 Collab., Seismic structure of the lithosphere between the East European Craton and the Carpathians from the net of CELEBRATION 2000 profiles in SE Poland, *Geol. Q.,* 2009, vol. 53, no. 1, pp. 141-158.

Komminaho, K., *Software Manual for Programs MODEL and XRAYS: a Graphical Interface for SEIS83 Program Package, Rep. 20, Univ.* Oulu, Dept. of Geophys., 1998.

Kostyukevych, A.S., Starostenko, V.I., and Stephenson, R.A., The full-wave images of the models of the deep lithosphere structures constructed according to DSS and CDP data interpretation, *Geofiz. Zh.*, 2000, vol. 22, no. 4, pp. 96–98.

Sollogub, V.B., *Litosfera Ukrainy* (Lithosphere of Ukraine), Kiev: Nauk. Dumka, 1986.

Sollogub, V.B. and Il'chenko, T.V., Wave field and seismic model, in *Litosfera Tsentral'noi i Vostochnoi Evropy. Geotraversy IV, VI, VIII* (Lithosphere of Central and Eastern Europe. Geotraverses IV, VI, VIII), Chekunov, V.B. Ed., Kiev: Naukova Dumka, 1988, pp. 128–132.

Środa, P., Czuba, W., Grad, M., Guterch, A., Tokarski, A., Janik, T., Rauch, M., Keller, G.R., Hegedűs, E., and Vozár, J., and CELEBRATION 2000 Collab., Crustal structure of the Western Carpathians from CELEBRATION 2000 profiles CEL01 and CEL04: seismic models and geological implication, *Geophys. J. Int.*, 2006, vol. 167, pp. 737–760. doi 10.1111/j.1365-246X.2006.03104.x

Starostenko, V.I., Kazanskii, V.I., Drogitskaya, G.M., et al., Relationship of the surface structures of Kirovograd ore region (Ukrainian Shield) with local heterogeneities of the crust and Moho topography, *Geofiz. Zh.*, 2007, vol. 29, no. 1, pp. 3–21.

Starostenko, V., Janik, T., Lysynchuk, D., Środa, P., Czuba, W., Kolomiyets, K., Aleksandrowski, P., Gintov, O., Omelchenko, V., Komminaho, K., Guterch, A., Tiira, T., Gryn, D., Legostaeva, O., Thybo, H., and Tolkunov, A., Mesozoic (?) lithosphere-scale buckling of the East European craton in Southern Ukraine: DOBRE-4 deep seismic profile, *Geophys. J. Int.*, 2013, vol. 195, pp. 740–766.

Zelt, C.A., *Software package ZPLOT, Cambridge: Univ.* Cambridge, Bullard Laboratories, 1994.

Translated by M. Nazarenko